

See discussions, stats, and author profiles for this publication at: <https://www.researchgate.net/publication/5328878>

# Design, Synthesis, and Biological Evaluation of Novel 3-Aryl-4-(1 H -indole-3yl)-1,5-dihydro-2 H -pyrrole-2-ones as Vascular Endothelial Growth Factor Receptor (VEGF-R) Inhibitors

ARTICLE in JOURNAL OF MEDICINAL CHEMISTRY · AUGUST 2008

Impact Factor: 5.45 · DOI: 10.1021/jm8001185 · Source: PubMed

---

CITATIONS

32

---

READS

38

10 AUTHORS, INCLUDING:



Dimitri Ott

University of Bayreuth

6 PUBLICATIONS 85 CITATIONS

SEE PROFILE



C. Schaechtele

ProQinase GmbH

94 PUBLICATIONS 3,444 CITATIONS

SEE PROFILE

## Design, Synthesis, and Biological Evaluation of Novel 3-Aryl-4-(1H-indole-3-yl)-1,5-dihydro-2H-pyrrole-2-ones as Vascular Endothelial Growth Factor Receptor (VEGF-R) Inhibitors

Christian Peifer,<sup>\*,§</sup> Roland Selig,<sup>§</sup> Katrin Kinkel,<sup>§</sup> Dimitri Ott,<sup>§</sup> Frank Totzke,<sup>‡</sup> Christoph Schächtele,<sup>‡</sup> Regina Heidenreich,<sup>†</sup> Martin Röcken,<sup>†</sup> Dieter Schollmeyer,<sup>||</sup> and Stefan Laufer<sup>§</sup>

Department of Pharmacy, Eberhard-Karls University, Auf der Morgenstelle 8, D-72076 Tübingen, Germany, ProQinase GmbH, Breisacherstrasse 117, D-79106 Freiburg, Germany, Department of Dermatology, Eberhard-Karls University, Liebermeisterstrasse 25, D-72076 Tübingen, Germany, and Department of Organic Chemistry, Johannes Gutenberg University Mainz, Duesbergweg 10-14, D-55099 Mainz, Germany

Received December 12, 2007

In this study we report on the design, synthesis, and biological evaluation of pyrrole-2-one **2** to be a highly potent VEGF-R2/3 inhibitor with IC<sub>50</sub> of 31/37 nM. The novel 3,4-diaryl-2H-pyrrole-2-ones were designed on the basis of the modeled binding mode of the corresponding 1H-pyrrole-2,5-dione (maleimide) VEGF-R2/3 inhibitor **1** indicating two H-bond ligand–protein interactions in the ATP pocket for the amide **2** but not for the isomer **3**. Flexible synthetic routes to 3,4-diaryl-2H-pyrrole-2-ones and structure–activity relationships for the compounds in a panel of 24 therapeutically relevant protein kinases (IC<sub>50</sub> values) are presented. Accordingly to the in vitro data, compounds **1** and **2** were found to possess highly potent antiangiogenic activities in the cellular HLMEC sprouting assay and also slightly induced apoptosis in HDMECs whereas **3** was determined to be significantly less active. Hence, the pyrrole-2-one moiety was dissected from the corresponding maleimide protein kinase inhibitor as a suitable key pharmacophore.

### Introduction

Vascular endothelial growth factor receptors (VEGF-Rs<sup>a</sup>) play pivotal roles in mediating the effects of hypoxia induced VEGFs not only on physiological angiogenesis but also on pathophysiological angiogenesis such as in pancreatic carcinomas, gastric carcinomas, colorectal carcinomas, breast cancer, lung cancer, prostate cancer, and melanoma.<sup>1</sup> The VEGF-R family consists of VEGF-R1 (also referred to as fms-like tyrosine kinase 1, Flt-1), VEGF-R2 (KDR), and VEGF-R3 (Flt-4), which have different binding specificities for VEGF members (VEGF-A to VEGF-E). VEGF-R1 is critical for physiological and developmental angiogenesis.<sup>2</sup> VEGF-R3 is restricted mainly to lymphatic endothelial cells,<sup>3,4</sup> whereas a low basic VEGF-R2 expression occurs on almost all endothelial cells. Despite this

diversity, VEGF-R2 seems to mediate at modulated high levels the majority of pathological angiogenic effects including microvascular permeability, endothelial cell differentiation, proliferation, invasion, and migration.<sup>5</sup> The importance of VEGF-R2 for the regulation of angiogenesis has been highlighted by the fact that homozygous knockout mice die at an early embryonic level, whereas the specific activation of VEGF-R2 alone by VEGF-E results in potent endothelial cell activity and angiogenesis.<sup>6</sup> At a molecular level of signal transduction, extracellular binding of VEGF-A or VEGF-E causes dimerization of the transmembrane VEGF-R2. Subsequently, the intracellular tyrosine kinase domains of VEGF-R2 autophosphorylate each other at different sites (Tyr<sup>951</sup>, Tyr<sup>1175</sup>, Tyr<sup>1214</sup>). Activated VEGF-R2 through these cascades triggers multiple intracellular downstream signaling pathways involving activation of phospholipase C  $\gamma$ -protein kinase C-Raf-MAP kinase pathways<sup>7</sup> resulting in proliferation of endothelial cells, whereas survival and migration are mediated via activation of PI3K/Akt and Src/focal adhesion kinase (FAK) pathways, respectively.<sup>8</sup> Taken together, VEGF-R2 situated at the top level of these cascades is working as a significant integrative “biochemical amplifier” of VEGF-A and VEGF-E signals and is considered to be a validated drug target in angiogenesis related diseases. Hence, a plethora of clinically effective strategies for its inhibition have been developed. These include neutralizing antibodies to VEGF or VEGF-Rs and small molecule tyrosine kinase inhibitors.<sup>6</sup>

### Small Molecule VEGF-R2 Inhibitors

Among protein kinases (PKs) as drug targets, tyrosine kinases such as VEGFR-2 play an outstanding role for the development of clinically effective inhibitors in oncology.<sup>5</sup> Since VEGF-R2 and the other PKs of the kinome use ATP as cofactor for the phosphorylation of proteins, they share a highly conserved ATP binding pocket that is the molecular binding site of most inhibitors. Many compounds that have been developed to

\* To whom correspondence should be addressed. Phone: 0049 7071 29 75278. Fax: 0049 7071 29 5037. E-mail: Christian.Peifer@uni-tuebingen.de.

<sup>§</sup> Department of Pharmacy, Eberhard-Karls University.

<sup>‡</sup> ProQinase GmbH.

<sup>†</sup> Department of Dermatology, Eberhard-Karls University.

<sup>||</sup> Johannes Gutenberg University Mainz.

<sup>a</sup> Abbreviations: AKT1, v-akt murine thymoma viral oncogene homologue 1 (PKB); ARK5, AMPK-related protein kinase 5 (NUAK1); Aurora, aurora kinase; B-RAF, v-raf murine sarcoma viral oncogene homologue B1; CDI, carbonyldiimidazole; CDK, cyclin-dependent kinase; CK, casein kinase; COT, mitogen-activated protein kinase kinase kinase 8 (MAP3K8); DDQ, 2,3-dichloro-5,6-dicyano-1,4-benzoquinone; EGF-R, epidermal growth factor receptor; EPHB, EPH receptor B; FAK, focal adhesion kinase; FLT3, fms-related tyrosine kinase 3; HDMEC, human dermal microvascular endothelial cells; HLMEC, human lung-derived microvascular endothelial cells; HMDS, hexamethyldisilazide; HOBT, hydroxybenzotriazole; HPI, hydrophobic pocket; HRIL, hydrophobic region II; IGF1-R, insulin-like growth factor 1 receptor; INS-R, insulin receptor; MET, met proto-oncogene (hepatocyte growth factor receptor); PDGF-R, platelet-derived growth factor receptor; PK, protein kinase; PLK1, polo-like kinase 1; PPA, polyphosphoric acid; SAK, serine/threonine-protein kinase (PLK4); SEM, 2-(trimethylsilyl)ethoxymethyl; SRC, v-src sarcoma (Schmidt–Ruppin A-2) viral oncogene homologue; TBAF, tetra-*n*-butylammonium fluoride; <sup>t</sup>BuOK, potassium *tert*-butoxide; TIE2, tunica interna endothelial cell kinase; TIPS, triisopropylsilyl; TMSCL, trimethylsilylchloride; VEGF-R, vascular endothelial growth factor receptor.

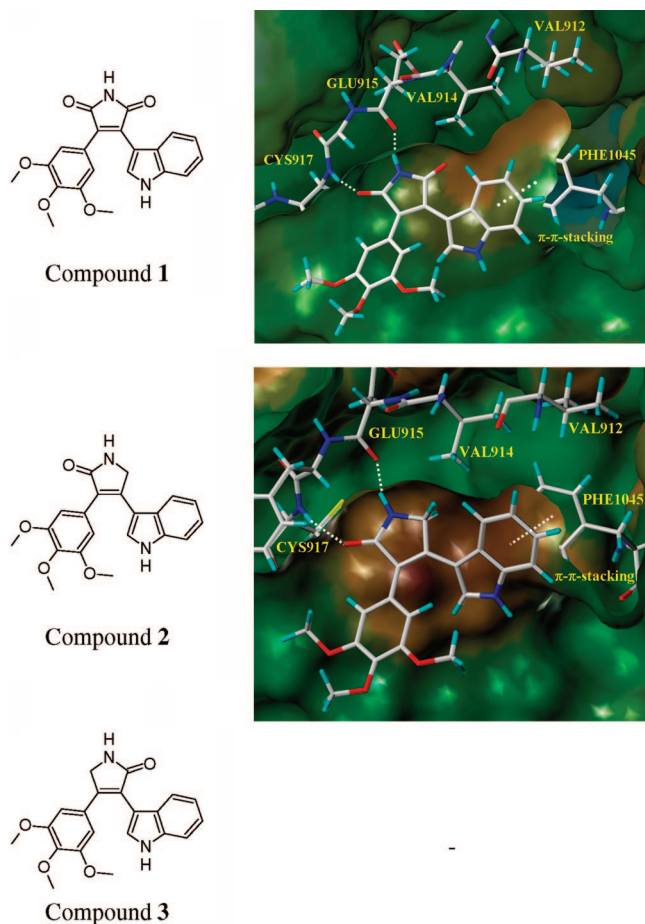


**Figure 1.** Crystallographically determined ATP-binding site of VEGF-R2 (pdb code 1Y6A)<sup>17</sup> and modelled binding modes of **1** and **2**. Key residues and hydrogen bonds are labeled. For compound **3** no rational binding mode in the ATP binding pocket of VEGF-R2 could be calculated.

selectively inhibit VEGF-R2 have also significant affinity for VEGF-R1 and VEGF-R3 as well as for other tyrosine kinase receptors such as the fibroblast growth factor receptor (FGFR),<sup>9</sup> epidermal growth factor receptors (EGFRs),<sup>10,11</sup> platelet derived growth factor receptors (PDGFR $\alpha/\beta$ ),<sup>12</sup> c-kit, and Flt-3 and for various other PKs.<sup>13</sup> Thus, the specificity of protein kinase inhibitors within the kinome is a key question and a robust evaluation of potency and selectivity is an essential part of drug discovery programs.<sup>14,15</sup>

In this paper we report on the design, synthesis, and biological evaluation of the 3-aryl-4-indolyl-2H-pyrrole-2-one **2** as a potent VEGF-R2 inhibitor with an IC<sub>50</sub> of 31 nM and strong in vivo activity in the HLMEC sprouting assay. We designed the novel pyrrole-2-ones derivatives on the basis of the rational binding mode for the highly active and selective inhibitor **1** (3-(1H-indole-3-yl)-4-(3,4,5-trimethoxyphenyl)-1,5-dihydro-2H-pyrrole-2-one) modeled in the ATP binding pocket of VEGF-R2 (Figure 1).<sup>16</sup> Herein, central hydrogen bonds to the hinge backbone carbonyl of Glu915 and to the backbone amine of Cys917 are formed. The indole ring is located in the hydrophobic region I with  $\pi$ - $\pi$  stacking interactions to Phe1045, whereas the trimethoxyphenyl moiety is situated in the hydrophobic region II.

Since, besides the NH-Glu915 in this calculated binding mode, only the 5' carbonyl oxygen and not the 2' oxygen of the maleimide moiety is involved in ligand-protein interactions to Cys917, we hypothesized that the corresponding 3,4-diaryl-2H-pyrrole-2-one scaffold was suitable as a pharmacophore to

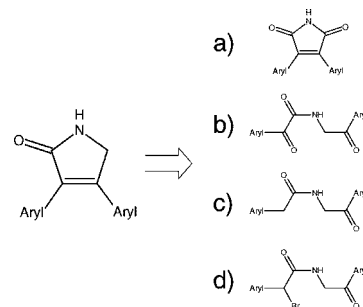


**Figure 2.** Retrosynthetic concepts for the preparation of 3,4-diaryl-2H-pyrrole-2-ones from the adequate precursors by (a) regioselective reduction of maleimides, (b) McMurry coupling, (c) aldol condensation (Knoevenagel-reaction), (d) intramolecular Wittig reaction.

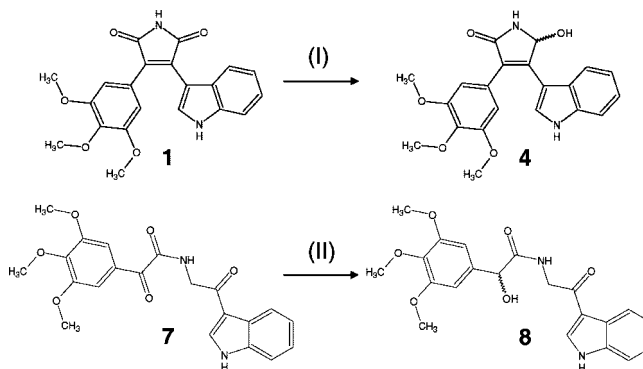


**Figure 3.** Modified Luche reduction of **1** yielded **4** as racemic mixture (I, ethanol, CeCl<sub>3</sub>, NaBH<sub>4</sub>). McMurry reaction of **7** resulted in a racemic mixture of **8** (besides undefined polymers) (II, THF, Ti (TiCl<sub>3</sub>), TMSCl, reflux).

also inhibit VEGF-R2/3. Accordingly, molecular modeling studies revealed a rational binding mode in the ATP pocket of VEGF-R2 comparable to **1** for 4-(1H-indole-3-yl)-3-(3,4,5-trimethoxyphenyl)-1,5-dihydro-2H-pyrrole-2-one (compound **2**) but not for the isomer 3-(1H-indole-3-yl)-4-(3,4,5-trimethoxyphenyl)-1,5-dihydro-2H-pyrrole-2-one (compound **3**, Figure 1).

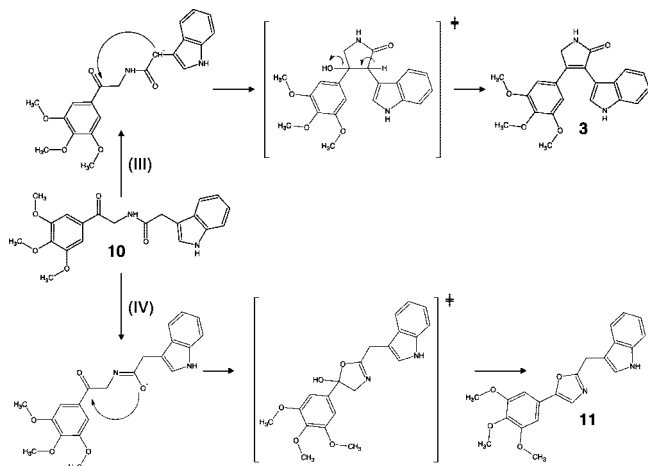
To prove this hypothesis, **2** and **3** possessing analogue substitution as compound **1** were synthesized and evaluated for their potency against VEGF-R2/3.

## Chemistry

Although many synthetic approaches toward symmetrically or asymmetrically substituted pyrrole-2-ones,<sup>18,19</sup> pyrrole-2,5-diones (maleimides),<sup>20–22</sup> and related carbazoles<sup>23–26</sup> exist, no adequate procedures for the flexible preparation of 3,4-aryl-(indole-3-yl)-2H-pyrrole-2-one have been reported. However, a retrosynthetic analysis of **2** and **3** revealed different possibilities for the flexible preparation of 3,4-diaryl-2H-pyrrole-2-one including a regioselective reduction of maleimides, strategies based on a McMurry coupling, an aldol reaction, and an intramolecular Wittig reaction (Figure 2).

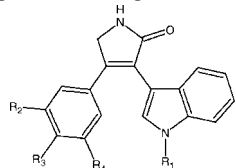
According to these concepts a modified Luche reduction<sup>27</sup> of **1** yielded **4**, but all further attempts to reduce the alcohol to the methylene moiety (**2**) failed.<sup>25,28,29</sup> Concerning the McMurry reaction,<sup>30</sup> we prepared precursor **7**, which was reacted under various coupling conditions,<sup>31,32</sup> but the ring closure for the pyrrole-2-one moiety did not perform and we obtained compound **8** as the main product in combination with polymeric tars (Figure 3).

The aldol condensation of **10** by use of the strong base <sup>t</sup>BuOK under reflux (thermodynamic conditions)<sup>33,34</sup> yielded the desired



**Figure 4.** Aldol condensation of **10** under thermodynamic Knoevenagel conditions (III, THF, <sup>t</sup>BuOK, reflux) yielded **3**, whereas kinetic conditions (IV, dichloromethane, 4 equiv of pyridine, 1 equiv of K<sub>2</sub>CO<sub>3</sub>, room temperature) yielded **11**.

**Table 1.** Substitution patterns of compounds **3**, **31**, **33**, and **35**

				
compd	R <sub>1</sub>	R <sub>2</sub>	R <sub>3</sub>	R <sub>4</sub>
<b>3</b>	H	OCH <sub>3</sub>	OCH <sub>3</sub>	OCH <sub>3</sub>
<b>31</b>	CH	OCH <sub>3</sub>	OCH <sub>3</sub>	OCH <sub>3</sub>
<b>33</b>	H	H	OCH <sub>3</sub>	H
<b>35</b>	CH <sub>3</sub>	H	OCH <sub>3</sub>	H

product **3** in good amounts. The reaction mechanism herein involves deprotonation of the benzylic position in **10** to generate a carbanion, which in turn attacks the carbonyl function to form the pyrrole-2-one ring by an E<sub>1cB</sub> mechanism. It is noteworthy that the use of the weaker bases pyridine and potassium carbonate at room temperature (kinetic conditions) yielded oxazole **11** by an aldol reaction of **10** (Figure 4).<sup>35,36</sup>

According to the straightforward strategy for the preparation of **3**, the analogue compounds **31**, **33**, and **35** were obtained from adequate precursors (Table 1). Thus, because the aldol strategy was successful, in this study the Wittig approach (Figure 2) was abandoned.

Interestingly, for the preparation of **2** the aldol condensation methodology via reaction of precursor **13** was initially not successful. In light of the established aldol mechanism for the reaction of **10** (to generate **3**) the complete loss of reactivity of isomeric **13** (to generate **2**) can be explained by the different pK<sub>a</sub> values in these molecules affecting the deprotonation of **13** compared to the isomer **10** (Figure 5). Because of the carbonyl function in 3' side chain position of the indole moiety, compound **13** is able to form a vinylogue amide system in which under the strong basic conditions the indole NH (pK<sub>aNH</sub> ≈ 13)<sup>37</sup> is deprotonated rather than the benzylic position (pK<sub>aCH</sub> ≈ 16). As a consequence of the indole NH deprotonation, the subsequently formed anion is delocalized over the vinylogue system, thereby deactivating the carbonyl reactivity that is necessary for the aldol condensation. However, reaction of **13** in polyphosphoric acid (PPA) led to compound **14** (Figure 5), the isomer of oxazole **11**.<sup>35</sup>

In order to avoid the indole NH deprotonation according to the tautomeric situation in **13** and to regain the required carbonyl reactivity, we introduced a variety of indole NH protecting groups to this molecule (Figure 6). Interestingly, for the triisopropylsilyl (TIPS) protected derivative we obtained compound **15** (Figure 6; structure of **15** has been proven by X-ray analysis<sup>38</sup>), which was not stable for further reactions. Herein, the tautomerization and unexpected subsequent protection of the indole 3' side chain oxygen in **15** confirm the deactivation of the indole 3' side chain carbonyl reactivity as discussed above. Furthermore, the phenylsulfonyl-protected compound **16** was immediately oxidized under the alkaline conditions to **17**. Albeit the mechanism for this reaction is still under investigation, we assume that the strong electron withdrawal effect of the phenylsulfonyl group facilitates the oxidation of the pyrrole-2-one methylene group. However, ring closure to the desired pyrrole-2-one derivative **19** under the thermodynamic Knoevenagel reaction conditions was successful for the 2-(trimethylsilyl)ethoxymethyl (SEM) protected species **18** (Figure 6).<sup>33</sup>

After successful achievement of the ring closure to pyrrole-2-one **19**, the subsequent removal of the SEM protecting group to generate **2** unexpectedly turned out to be quite difficult. Even if SEM deprotection of related indole derivatives commonly achieved by TBAF (Bu<sub>4</sub>NF) has been reported to proceed without further complications<sup>25,34</sup> in this case, the removal was a challenge. The mechanism of SEM cleavage usually involves a hemiaminal that eliminates formaldehyde (commonly sequestered by bases such as ethylenediamine<sup>39</sup>) to yield the unsubstituted indole NH. Unfortunately in our case all attempts involving fluoride induced cleavage of SEM in **19** using various solvents and conditions failed.<sup>40</sup> Instead of SEM cleavage by TBAF under alkaline conditions, an oxidation of **19** to **19a** (possessing the pyrrole-2,5-dione moiety) occurred, as also seen in related compounds.<sup>25</sup> In particular, the use of bases such as ethylenediamine typically resulted in oxidation and destruction of **19** and gave complex mixtures of red tars. Thus, as already seen for compound **17** the methylene bridge in the 3,4-diaryl-1,5-dihydro-2H-pyrrole-2-one moiety of **19** was found to be susceptible for oxidation particularly under basic conditions. Interestingly, SEM cleavage at the pyrrole-2,5-dione core proceeded successfully by refluxing **19a** in TBAF, DMF, and ethylenediamine to yield **1** (yield 70%).

This prompted us to develop a method for SEM cleavage under acidic conditions for the deprotection of molecule **19**. However, refluxing SEM-protected **19** in methanol with catalytic amounts of HCl quantitatively resulted in **21** formally possessing the MOM protection (Figure 7). The mechanism for this reaction can be explained via conventional elimination of ethene from **19** yielding the hemiaminal **20** as intermediate, which reacts, consecutively and via proton catalysis, with an excess of alcoholic solvent to generate the methoxyaminal. Accordingly, the reaction of **19** in various alcohols gave the corresponding derivatives **22–26** (Figure 7). Interestingly, reaction of HCl with **19** in *tert*-butyl alcohol as solvent gave a mixture of three main products that were separated by flash chromatography to yield **2** (10%), **20** (46%), and **24** (16%, Figure 7). Thus, it is noteworthy that in this study compound **2** could be generated indirectly from **19** under acidic conditions. Furthermore, **2** was also generated from **20**, eliminating formaldehyde by the use of sodium methanolate in dry methanol.

Compound **29** was synthesized via the precursors **27** and **28** (Figure 8), wherein the 4-ethyl-2,2-dimethyl-1,3-dioxolane side chain was used elegantly as a "protected protecting group" for



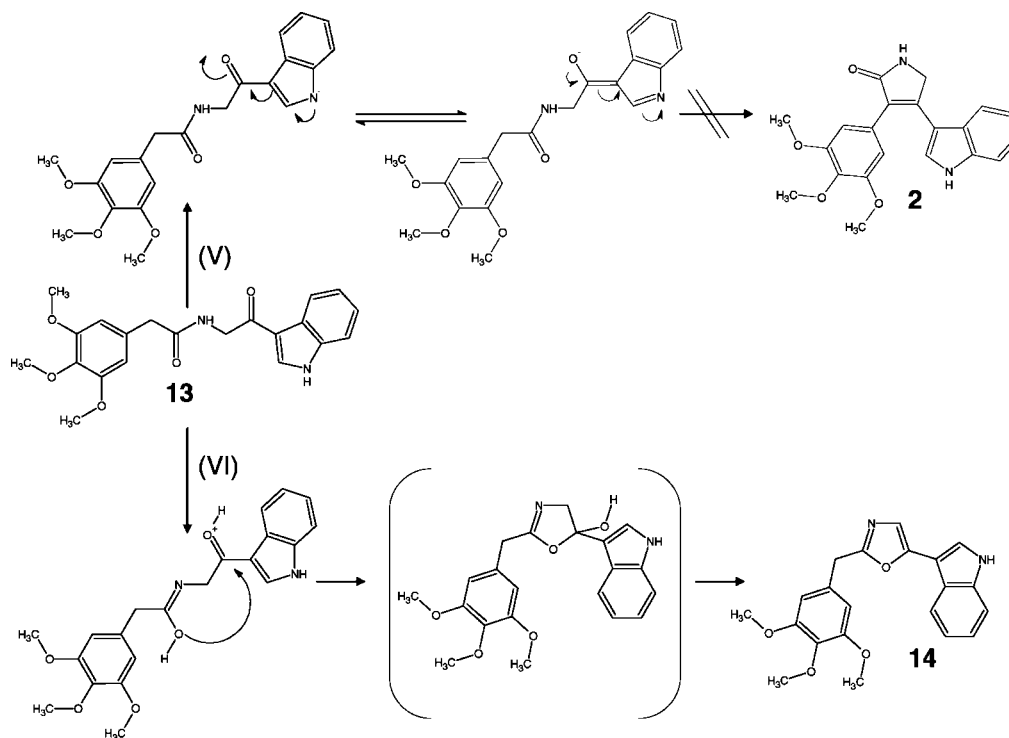


**Figure 5.** Aldol condensation of **13** under thermodynamic Knoevenagel conditions (V, THF, <sup>t</sup>BuOK, reflux) was not successful because of the deprotonation of indole NH. The tautomeric situation completely deactivates the carbonyl reactivity necessary for ring closure. Under acidic conditions (VI, PPA, 80 °C), the oxazole **14** was formed.

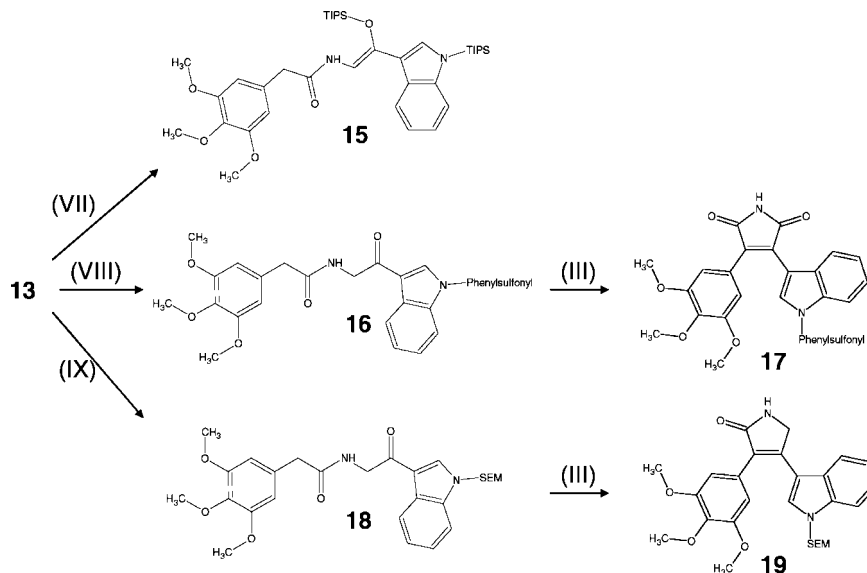


**Figure 6.** Strategies for the introduction of protecting groups to compound **13** (VII, THF, NaH, TIPSCl; VIII, EtOH, KOH, benzoysulfonylchloride; IX, THF, NaHMDS, SEMCl; III, THF, <sup>t</sup>BuOK, reflux).

the indole NH accordingly to the requirements for the Knoevenagel condensation (as discussed above).

### Biological Evaluation and Discussion

The pyrrole-2-ones of this study and maleimide **1** have been evaluated in vitro for their biological activity in a panel of 24 therapeutically relevant PKs including VEGF-R2/3 (Table 2). Consistent with the molecular modeling in the ATP pocket of VEGF-R2 (Figure 1), compounds **2** and **1**<sup>16</sup> were found to potently inhibit these receptor tyrosine kinases (**2** VEGF-R2 IC<sub>50</sub> = 0.031 μM; VEGF-R3 IC<sub>50</sub> = 0.037 μM). In contrast to compound **2** the isomer **3** showed a significant weaker inhibition

of VEGF-R2 (IC<sub>50</sub> = 11 μM) and VEGF-R3 (IC<sub>50</sub> = 9.4 μM). Hence, these data strongly confirm the calculated ligand–protein interactions of **2** in particular for the lactame moiety, which was supposed to address the amino acids Glu915 and Cys917. However, the lactame **2** was determined to inhibit VEGF-R2/3 (and the other kinases of this panel) approximately 10-fold less than maleimide **1**. This moderate loss of activity may be due to the lower polarization of the NH in amide **2** compared to imide **1** and a subsequently weaker H-bond to the carbonyl of Glu915 in VEGF-R2/3.

On the other hand, although **3** (as well as **31**, **33**, and **35**) compared with the isomer **2** showed the expected reduction of

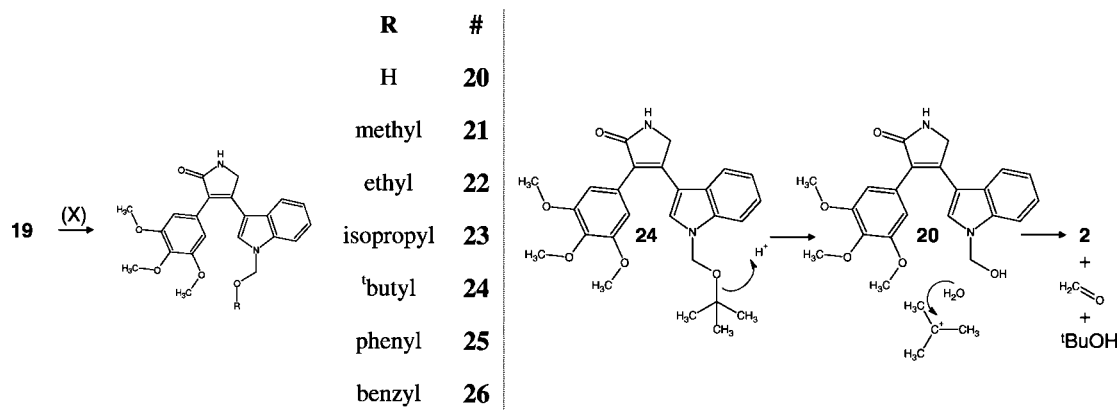


**Figure 7.** Reaction of **19** in different alcohols and catalytic amount of HCl generated the corresponding compounds **21–26** (X, particular alcohol as solvent, catalytic amounts of HCl, reflux). Because of the *tert*-butylcarbocation as a leaving group, hemiaminal **20** was found as an unstable intermediate in the reaction of **19** with *t*-BuOH, and **2** was subsequently obtained from **20** by the elimination of formaldehyde.

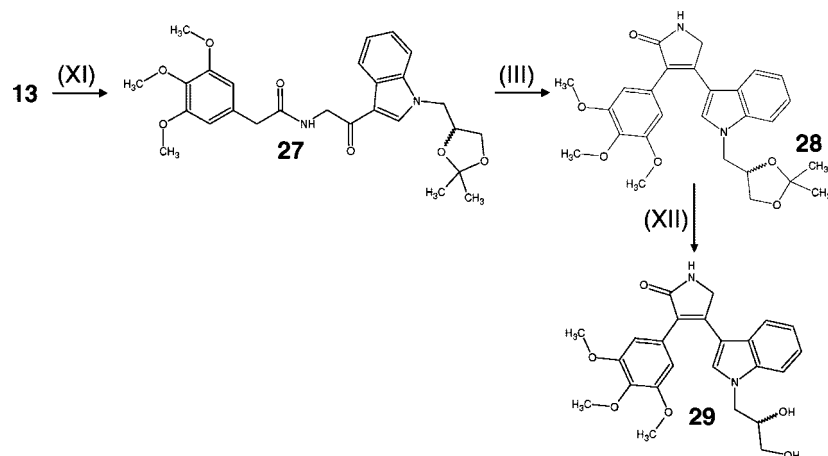


**Figure 8.** Synthesis of **29** via protected **27**, ring closure to **28**, and deprotection to yield **29** (XI, DMF,  $K_2CO_3$ , 4-(bromomethyl)-2,2-dimethyl-1,3-dioxolane, reflux; III, THF, *t*-BuOK, reflux; XII, dichloromethane, catalytic amount of HCl).

activity against VEGF-R2/3, we found considerable inhibition of ARK5, AuroraA/B, and SAK in the single digit micromolar range for compound **3** and for the derivatives of this isomer, depending on the aryl substitution. Interestingly, FLT3 was inhibited by **1** with an  $IC_{50}$  of 270 nM, but the two isomers **2** and **3** were found to have both a similar  $IC_{50}$  in the low micromolar range (**2**  $IC_{50}$  = 6.1  $\mu M$ ; **3**  $IC_{50}$  = 2.2  $\mu M$ ). These data indicate that the maleimide moiety in **1** presumably interacts with the hinge region of FLT3 by the NH as well as both oxygens, thereby accounting for the nanomolar potency. Compared to the nanomolar inhibitors **1** and **2**, the 2'-hydroxyl function in **4** significantly reduced the biological activity for VEGF-R2/3 to the micromolar range (**4**  $IC_{50}$  = 5.9  $\mu M$ /3.4  $\mu M$ ) and abolished the activity against many of the other kinases in the panel. Since in this study compound **4** had been tested in the kinase assays as a 2'-racemic mixture, it is not possible to describe a clear stereochemical SAR for this position.

The unsubstituted indole-NH in compound **2** was found to be essential for potent inhibition of VEGF-R2/3. This result goes parallel with the SAR of **1** at VEGF-R2/3 where the free indole-NH was found to be relevant for high affinity too.<sup>20</sup> Thus, as previously described,<sup>16</sup> we suppose a similar water mediated ligand–protein interaction for the indole NH of **2** to the ribose pocket (Arg1030 and Asn1031) of VEGF-R2/3. Accordingly, the substituted derivatives **19** and **21–26** showed  $IC_{50}$  values only in the micromolar range (Table 2). However, within this series compound **26** (VEGF-R2/3  $IC_{50}$  = 1.6/1.7  $\mu M$ ), possess-

ing a benzyloxymethylene substitution at the indole nitrogen, showed promising specificity for VEGF-R2/3 in the kinase panel.

Consistent with the proposed binding mode of compound **2** in the ATP pocket of VEGF-R2 (Figure 1), we designed compound **29** possessing a dihydroxy-functionalized side chain that was intended to interact with Arg840 of the glycine-rich loop (Figure 9). In light of the chiral 2'-hydroxyl function of **29**, molecular modeling showed suitable ligand–protein interactions for the propylene glycol *S*-enantiomer but not for the corresponding *R*-enantiomer (not shown). However, the *in vitro* inhibitory activity for racemic **29** at VEGF-R2/3 ( $IC_{50}$  = 4.2  $\mu M$ /2.5  $\mu M$ ) was determined to be in the micromolar range, as also seen for the other indole N-substituted derivatives **19–26** (and **28**). Although the defined enantiomers of **29** have not been tested, the weak  $IC_{50}$  values of racemic **29** for VEGF-R2/3 comparable to protected **28** indicate that no additional H-bond to the protein was formed by the hydroxy moieties of **29**. Thus, in contrast to the calculated binding mode of **29** in the ATP pocket of VEGF-R2, this optimization strategy was not successful and may be due to different reasons. First, protein kinase domains such as the glycine-rich loop and the DFG motif are highly flexible while the crystal structure used for modeling reflects only one specific protein conformation,<sup>41</sup> which was presumably not realistic for the binding of **29** in VEGF-R2. Second, the relatively rigid alkyl side chain of **29** bearing the hydroxy functions may not provide the molecule with the

**Table 2.** IC<sub>50</sub> Values (μM) up to 50 μM Test Compounds in This Study in an Assay Panel of 24 Therapeutically Relevant PKs of the Kinome<sup>a</sup>

C p d #	A A B- C C E E E I S												V V		P							
	A	u	u	R	D	D	E	E	E	F	G	S	E	E	F	I	M	D	S	T	C	
	R	R	R	A	K	K	G	P	R	A	F	R	G	G	L	N	E	G	A	I	O	
	K	o	o	F-	2/	4/	F-	H	B	B	K	1-	F-	F-	T	S-	T	F	K	E	T	
	5	a	a	V	Cyc	Cyc	R	B	B	K	R	C	R	R	3	R		R-		2	T	
	A	B		E	A	D1		4	2				2	3				β				
1	43	5.4	17	40	6.9	14	16	5.1	26	0.65	13	21	0.0025	0.005	0.27	16	35	0.68	0.99	0.74	-	
2	-	16	46	-	-	-	23	-	-	9.5	22	14	0.031	0.037	6.1	43	-	11	10	5.2	32	
3	1.8	3.2	2.1	-	-	30	-	-	-	-	-	41	11	9.4	2.2	-	-	-	7.7	34	-	
4	-	-	-	-	-	-	-	-	-	-	-	-	5.9	3.4	44	-	-	-	-	-	-	
19	-	-	-	-	-	-	22	44	-	-	8.7	4.5	3.1	5.6	34	-	-	-	-	26	-	
21	-	-	-	-	-	-	-	-	-	35	-	-	2.3	3.2	25	-	-	-	-	25	-	
22	-	29	-	-	-	-	-	-	-	28	-	40	5.3	3.6	-	-	-	-	35	24	-	
23	-	33	-	-	-	-	-	-	-	27	-	29	5.2	5.3	-	-	-	-	44	11	-	
24	-	30	43	38	23	27	9.0	20	25	28	7.7	4.4	4.4	4.8	20	27	29	38	28	11	9.6	
25	-	6.5	20	-	20	44	-	-	37	43	-	49	1.5	2.5	-	44	45	-	9.0	1.7	40	
26	-	-	-	-	-	-	14	37	36	40	18	9.1	1.6	1.7	36	-	-	-	-	11	-	
28	-	-	-	-	-	-	-	-	-	-	-	-	8.0	3.2	-	-	-	-	23	31	-	
29	34	47	-	-	-	-	-	-	-	-	-	-	4.2	2.5	3.0	-	-	40	16	25	-	
31	4.9	3.2	9.8	50	42	40	-	-	-	50	-	-	15	11	5.0	47	-	45	9.2	-	-	
33	2.0	16	4.9	-	-	35	-	-	-	-	-	-	13	8.7	9.9	-	-	-	12	-	-	
35	3.6	-	-	-	-	-	-	-	-	-	-	39	31	18	14	-	-	-	46	48	-	

indicates IC<sub>50</sub> values < 1·10<sup>-7</sup> (M)

indicates IC<sub>50</sub> values 1·10<sup>-7</sup> – 9.9·10<sup>-7</sup> (M)

indicates IC<sub>50</sub> values 1·10<sup>-6</sup> – 9.9·10<sup>-6</sup> (M)

-

 indicates no significant inhibition up to 5 ·10<sup>-5</sup> (M)

	indicates IC <sub>50</sub> values < 1·10 <sup>-7</sup> (M)		indicates IC <sub>50</sub> values 1·10 <sup>-6</sup> – 9.9·10 <sup>-6</sup> (M)
	indicates IC <sub>50</sub> values 1·10 <sup>-7</sup> – 9.9·10 <sup>-7</sup> (M)	-	indicates no significant inhibition up to 5·10 <sup>-5</sup> (M)

<sup>a</sup> None of the compounds significantly inhibited AKT1, CK2-A1, and PLK1 up to 50 μM. As a parameter for assay quality, the Z'-factor for the low and high controls of each assay plate (n = 8) was used (for details, see Supporting Information).

capability of adopting the optimal conformation necessary for additional H-bond interactions to Arg840 in the glycin-rich loop of VEGF-R2.<sup>42</sup> Taken together, accurate and actual docking with protein kinases and inhibitors remains challenging.<sup>43</sup>

### Cellular in Vitro Characterization

Recent data show that multikinase inhibitors are clinically more effective for tumor therapy than single targeting compounds.<sup>44</sup> Even though the data of **2** determined so far show potent in vitro efficiency against VEGF-R2/3 and specificity over the other 22 PKs involved in the panel (Table 2), cellular in vitro studies are needed to analyze the efficacy of such compounds on receptor functioning. In light of the nanomolar potency of **1** and **2** and the significantly reduced activity of **3** against isolated VEGF-R2/3, these compounds have been assayed in an endothelial cell sprouting assay using human lung derived microvascular endothelial cells (HLMVEC) in order to reveal their antiangiogenic activity (Figures 10 and 11). In line

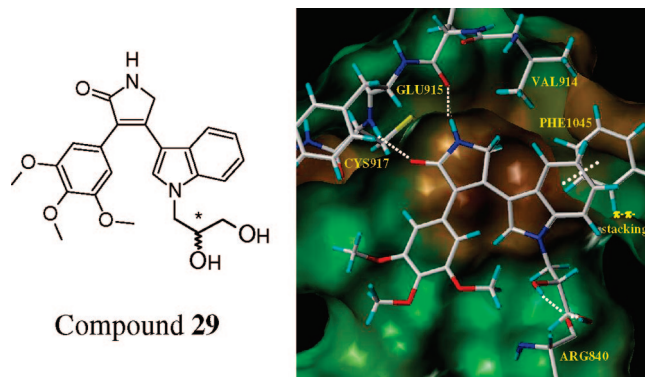


**Figure 9.** Crystallographically determined ATP-binding site of VEGF-R2 (PDB code 1Y6A)<sup>17</sup> and modelled binding mode of the S-enantiomer of **29**. Key residues and hydrogen bonds are labeled.

with the in vitro SAR data for VEGF-R, compounds **1** (81% inhibition) and **2** (88% inhibition) actually showed strong

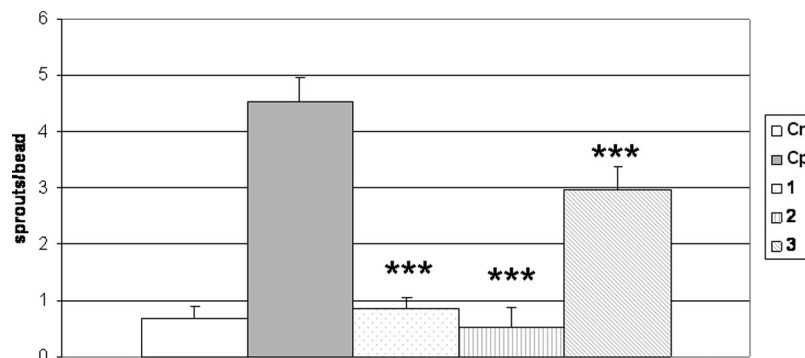


**Figure 10.** Antiangiogenic activity of compounds **1–3** at a concentration of 1.3  $\mu\text{M}$  in the HLMEC sprouting assay presented as sprouts/bead  $\pm$  SD (for each experiment  $n = 18$ ). Cn = control negative without VEGF stimulation:  $0.69 \pm 0.22$  sprouts/bead. Cp = control positive with 20 ng/mL VEGF stimulation:  $4.54 \pm 0.45$  sprouts/bead. Compound **1**:  $0.86 \pm 0.2$  sprouts/bead. Compound **2**:  $0.52 \pm 0.36$  sprouts/bead. Compound **3**:  $2.98 \pm 0.41$  sprouts/bead. Statistical analysis was performed by using GraphPad InStat3 software. ANOVA, Tukey–Kramer test, and Bonferroni test showed the results of compounds **1–3** to be highly significant compared to Cp (\*\*\*,  $p < 0.001$ ). Compound **1** vs **2** was not significant ( $p > 0.05$ ). Compounds **1** and **2** vs **3** were highly significant (\*\*\*,  $p < 0.001$ ).

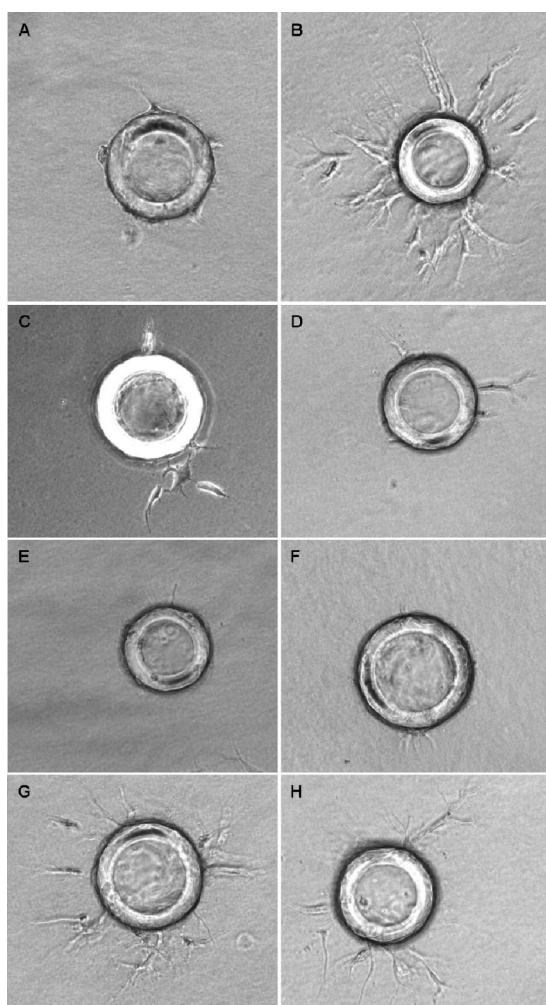


**Figure 11.** Antiangiogenic activity of compounds **1–3** in the HLMEC sprouting assay: (A) negative control, no VEGF stimulation; (B) positive control, stimulation with 20 ng/mL VEGF; (C) 1.3  $\mu\text{M}$  **1** and 20 ng/mL VEGF; (D) 2.6  $\mu\text{M}$  **1** and 20 ng/mL VEGF; (E) 1.3  $\mu\text{M}$  **2** and 20 ng/mL VEGF; (F) 2.6  $\mu\text{M}$  **2** and 20 ng/mL VEGF; (G) 1.3  $\mu\text{M}$  **3** and 20 ng/mL VEGF; (H) 2.6  $\mu\text{M}$  **3** and 20 ng/mL VEGF.

antiangiogenic potency at 1.3  $\mu\text{M}$  whereas compound **3** (34% inhibition) was significantly less active. The concentration range of the compounds for effective inhibition of HLMEC sprouting was dose dependent, as determined by titration experiments in this assay (data not shown; the results of **1–3** at 2.6  $\mu\text{M}$  are

presented in Supporting Information). Furthermore, at 1.3  $\mu\text{M}$  the derivatives **19** (30%  $\pm$  13% inhibition), **21** (42%  $\pm$  7% inhibition), and **25** (41%  $\pm$  4% inhibition) blocked the HLMEC sprouting less efficiently than highly active **2**. These results are also in accordance with their reduced in vitro VEGF-R activity.

Interestingly, although **2** compared to **1** has been determined to be approximately 10-fold less active in vitro against VEGF-R2/3 (Table 2), compound **2** reduced the sprouting of HLMECs down to the negative control level slightly more potent than **1**, and yet this difference was not significant (Figures 10 and 11). This effect may be due to different reasons. First, since maleimides have been reported to possess both poor water solubility and poor cellular bioavailability,<sup>45</sup> these parameters are presumably limiting for maleimide **1** but less for the lactame **2** to reach their cellular target(s). Second, further PK(s) involved in the angiogenic signaling process may be blocked more potently by **2** than by **1**, even though these PK(s) were not detected in our 24 kinase profiles. An enhanced panel of PKs to profile the compounds will be used in new experiments to address this question.

Since VEGF-R inhibition may result in considerable apoptosis<sup>46</sup> of endothelial cells (EC), we investigated if compounds **1–3** could induce apoptosis in EC such as human dermal microvascular endothelial cells (HDMEC). Herein, the compounds were tested at the antiangiogenic effective concentrations of 1.3 and 2.6  $\mu\text{M}$  compared to staurosporine<sup>47</sup> as a positive control (Figure 12).

At an antiangiogenic effective concentration of 1.3  $\mu\text{M}$ , compounds **1** (22.4  $\pm$  10.8%) and **2** (25.0  $\pm$  7.6%) both slightly increased the apoptosis rate compared to the negative control. At a concentration of 2.6  $\mu\text{M}$ , compound **2** significantly induced apoptosis (42.1%  $\pm$  8.8%), although this compound was not as potent as staurosporine, a widely unselective PK inhibitor.<sup>15</sup> As expected, compound **3** showed no significant induction of apoptosis at both concentrations. Taken together, in light of the considerable antiangiogenic effect of **2** in the sprouting assay at 1.3  $\mu\text{M}$ , it is remarkable that this concentration does not significantly induce apoptosis in endothelial cells.

## Conclusion

Novel regioselective substituted 3,4-diaryl-2*H*-pyrrole-2-ones were rationally designed, synthesized and subsequently evaluated as VEGF-R2/3 inhibitors. As a highly active and selective VEGF-R2/3 inhibitor with IC<sub>50</sub> values of 31/37 nM against the isolated enzymes compound **2** was also determined to potently



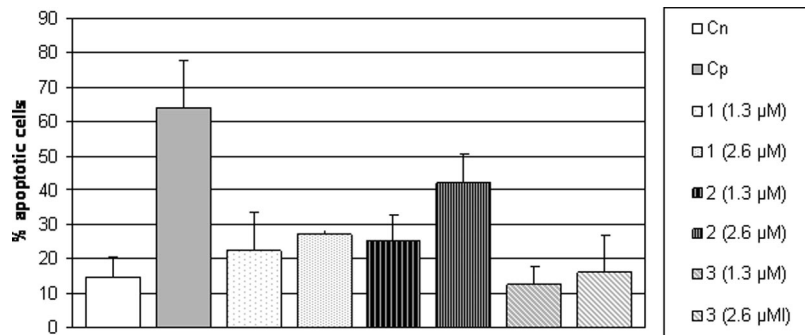


**Figure 12.** Dose dependent induction of apoptosis of compounds **1–3** in the HDMEC assay after 24 h of incubation represented as percent apoptotic cells  $\pm$  SD (for each experiment  $n = 3$ ). Cn = control negative,  $14.4 \pm 6.0\%$ . Cp = control positive,  $2.1 \mu\text{M}$  staurosporine after 5 h,  $63.9 \pm 13.8\%$ .

block angiogenesis in the HLMEC sprouting assay at a concentration of  $1.3 \mu\text{M}$  and to slightly induced apoptosis in the HDMEC assay at a concentration of  $2.6 \mu\text{M}$ . Thus, in light of the high in vitro activity and selectivity and also being bioavailable in the cellular models compound **2** may have potential for clinical development as an antiangiogenic drug.

## Experimental Section

**Chemistry.** Infrared spectra were recorded on a “Perkin Elmer Spectrum one” infrared spectrophotometer.  $^1\text{H}$  (200 MHz, digital resolution of 0.3768 Hz) and  $^{13}\text{C}$  (50 MHz, digital resolution of 1.1299 Hz) NMR were recorded on a Bruker AC 200. The data are reported as follows: chemical shift in ppm from  $\text{Me}_4\text{Si}$  as external standard, multiplicity, and coupling constant (Hz). GC/MS was performed on a HP6890 series system. EI mass spectra were recorded on a Varian MAT 311A (70 eV). HRMS and FD mass spectra were recorded on a MAT-95 (Finnigan). For clarity only the highest measured signal is given for FD mass spectra. Melting points/decomposition temperatures were determined on a Büchi apparatus according to Dr. Tottoli and are uncorrected. X-ray structure determination was performed on a CAD4-Enraf-Nonius using  $\text{Cu K}\alpha$  radiation with graphite monochromator. Where appropriate, column chromatography was performed for crude precursors with Merck silica gel 60 (0.063–0.200 mm) or Acros organics silica gel (0.060–0.200 mm, pore diameter of  $\sim 60$  nm). Column chromatography for test compounds was performed using a La-flash-System (VWR) with Merck silica gel 60 (0.015–0.040 mm) or RP8 columns. The progress of the reactions was monitored by thin-layer chromatography (TLC) performed with Merck silica gel 60 F-245 plates. Where necessary, reactions were carried out in a nitrogen atmosphere using  $4 \text{ \AA}$  molecular sieves. All reagents and solvents were obtained from commercial sources and used as received (THF was used after distillation over  $\text{K/benzophenone}$ ). Reagents were purchased from Sigma-Aldrich Chemie, Steinheim, Germany; Lancaster Synthesis, Mühlheim, Germany; or Acros, Nidderau, Germany.

HPLC analysis was performed on a Hewlett-Packard HP 1090 series II using a Thermo Betasil C8 ( $150 \mu\text{m} \times 4.6 \text{ mm}$ ) column (mobile phase flow  $1.5 \text{ mL/min}$ , gradient  $\text{KH}_2\text{PO}_4$  buffer, pH 2.3/ methanol, UV detection at 230/254 nm). A table summarizing the purity of key target compounds can be found in Supporting Information.

Routine experimental and NMR data are given in Supporting Information.

**General Method for Preparing Substituted Pyrrole-2-one Derivatives by Thermodynamic Knoevenagel Condensation.** A typical procedure (exemplified by the preparation of compound **19**) is as follows. A dry three-necked round-bottom flask was charged through a septum under argon with 1 mmol of a 20% (w/w) solution of  $t\text{BuOK}$  in THF and diluted with an additional 10 mL of dry THF. This mixture was heated to  $80^\circ\text{C}$  at which temperature a solution of 1 mmol of **18** in 10 mL of dry THF was added all at

once. The mixture immediately changed to deep-red and was stirred under reflux for 15 min (reaction progress monitored by TLC) when the starting material disappeared. The mixture was cooled in an ice bath and quenched with 1 mL of 10% HCl. The mixture was extracted by ethyl acetate and washed with brine. The organic phase was dried over  $\text{Na}_2\text{SO}_4$  and evaporated. The product **19** was purified by flash chromatography on silica gel using a gradient of ethyl acetate/ethanol (chromatogram see Supporting Information for details).

**3-(1H-Indol-3-yl)-4-(3,4,5-trimethoxyphenyl)-1H-pyrrole-2,5-dione (1).** The compound was prepared as described previously.<sup>20</sup> HRMS  $m/z = 378.12088$ , calculated  $378.121541$ ; purity HPLC 98.7%,  $t_R = 7.882$  min; mp  $245.8^\circ\text{C}$ .

**4-(1H-Indol-3-yl)-3-(3,4,5-trimethoxyphenyl)-1,5-dihydro-2H-pyrrole-2-one (2).** The compound was obtained after purification by flash chromatography from reaction mixture described for compound **20**, yielding 10% (70 mg) of **2** as a pale-white solid.

Alternative preparation of **2** is as follows. An amount of 400 mg (1 mmol) of **20** was dissolved under argon in 10 mL of dry methanol. To the mixture 100  $\mu\text{L}$  of a 0.5 M NaMeOH solution in methanol was added and stirred for 20 min. The mixture was cooled in an ice bath when 1 mL 10% HCl was added. The mixture was extracted by ethyl acetate and washed with brine. The organic phase dried over  $\text{Na}_2\text{SO}_4$  and evaporated. The product was purified by flash chromatography on silica gel using ethyl acetate and 10% ethanol to yield 47% (170 mg, 0.47 mmol) of **2**. LC–MS for  $\text{C}_{21}\text{H}_{20}\text{N}_2\text{O}_4$ , 365.1  $[\text{M} + \text{H}^+]$ , 363.0  $[\text{M} - \text{H}^+]$ ; mp  $131.8^\circ\text{C}$ ; HRMS  $m/z = 364.14069$ , calculated  $364.142281$ ; purity HPLC 97.9%,  $t_R = 5.199$  min. The crystal structure of **2** has been proven by X-ray analysis: CAD4 Enraf Nonius,  $\text{Cu K}\alpha$ , SIR-92, SHELXL-97, CCDC No. 680816. Further details of the crystal structure analysis are available in Supporting Information.

**3-(1H-Indol-3-yl)-4-(3,4,5-trimethoxyphenyl)-1,5-dihydro-2H-pyrrole-2-one (3).** The compound was prepared from 0.78 mmol of **10** following a general procedure. Yield after flash chromatography purification was 63% (0.49 mmol) as a fawn solid. FAB–MS for  $\text{C}_{21}\text{H}_{20}\text{N}_2\text{O}_4$ , 364.9  $[\text{M}^{++}]$ ; mp  $217.0^\circ\text{C}$ ; HRMS  $m/z = 364.14100$ , calculated  $364.142281$ ; purity HPLC 97.5%,  $t_R = 5.285$  min.

**5-Hydroxy-4-(1H-indol-3-yl)-3-(3,4,5-trimethoxyphenyl)-1,5-dihydro-2H-pyrrole-2-one (4).** LC–MS for  $\text{C}_{21}\text{H}_{20}\text{N}_2\text{O}_5$ ,  $^{**}382$   $[\text{M} + \text{H}]^+$ ; mp  $>250^\circ\text{C}$  dec; HRMS  $m/z = 380.13819$ , calculated  $380.137191$ ; purity HPLC 98.0%,  $t_R = 5.356$  min. Crystal structure of **4** has been proven by X-ray analysis: CAD4 Enraf Nonius,  $\text{Cu K}\alpha$ , SIR-92, SHELXL-97, CCDC No. 680817. Further details of the crystal structure analysis are available in Supporting Information.

**Oxo(3,4,5-trimethoxyphenyl)acetic Acid (5).**<sup>48</sup> LC–MS for  $\text{C}_{11}\text{H}_{12}\text{O}_6$ , 239  $[\text{M} - \text{H}]^+$ ; mp  $148.7^\circ\text{C}$ .

**N-[2-(1H-Indol-3-yl)ethyl]-2-oxo-2-(3,4,5-trimethoxyphenyl)-acetamide (6).** GC–MS for  $\text{C}_{21}\text{H}_{22}\text{N}_2\text{O}_5$ , 382  $[\text{M}]^+$ ; mp  $211.9^\circ\text{C}$ . **Caution!** The mixture must be absolutely free of water! If water was involved in this reaction, the salt 2-(1H-indol-3-yl)ethanaminium-oxo(3,4,5-trimethoxyphenyl)acetate (**6a**) was obtained

in our study. Crystal structure of **6a** has been proven by X-ray analysis: CAD4 Enraf Nonius, Cu K $\alpha$ , SIR-92, SHELXL-97, CCDC No. 680818. Further details of the crystal structure analysis are available in Supporting Information.

**N-[2-(1*H*-Indol-3-yl)-2-oxoethyl]-2-oxo-2-(3,4,5-trimethoxyphenyl)acetamide (7)**. EI-MS for C<sub>21</sub>H<sub>20</sub>N<sub>2</sub>O<sub>6</sub>, 396 [M]<sup>+</sup>; mp 194.3 °C.

**N-[2-(1*H*-Indol-3-yl)-2-oxoethyl]-2-hydroxy-2-(3,4,5-trimethoxyphenyl)acetamide (8)**. LC-MS for C<sub>21</sub>H<sub>22</sub>N<sub>2</sub>O<sub>6</sub>, 397 [M - H]<sup>+</sup>; mp 175.0 °C.

**1-Bromo-2-oxo-2-(3,4,5-trimethoxyphenyl)ethanaminium Bromide (9)**. The compound was prepared according to the literature.<sup>49</sup> FAB-MS for C<sub>11</sub>H<sub>16</sub>NO<sub>4</sub>, 226.1 [M<sup>+</sup>] (-bromide); mp 236.0 °C.

**2-(1*H*-Indol-3-yl)-N-[2-(3,4,5-trimethoxyphenyl)-2-oxoethyl]acetamide (10)**. FAB-MS for C<sub>21</sub>H<sub>22</sub>N<sub>2</sub>O<sub>5</sub>, 383.2 [M + H]<sup>+</sup>; mp 125.7 °C.

**3-[[5-(3,4,5-Trimethoxyphenyl)-1,3-oxazol-2-yl]methyl]-1*H*-indole (11)**. The compound was obtained following the procedure of method B for the preparation of **10**. FAB-MS for C<sub>21</sub>H<sub>20</sub>N<sub>2</sub>O<sub>4</sub>, 364.1 [M<sup>+</sup>]; mp 138.0 °C; HRMS *m/z* = 364.142 05, calculated 364.142 281; purity HPLC 98.8%, *t*<sub>R</sub> = 9.100 min. Crystal structure of **11** has been proven by X-ray analysis: CAD4 Enraf Nonius, Cu K $\alpha$ , SIR-92, SHELXL-97, CCDC No. 680819. Further details of the crystal structure analysis are available in Supporting Information.

**N-[2-(1*H*-Indol-3-yl)ethyl]-2-(3,4,5-trimethoxyphenyl)acetamide (12)**. GC-MS for C<sub>21</sub>H<sub>24</sub>N<sub>2</sub>O<sub>4</sub>, 368 [M<sup>+</sup>]; mp 120.1 °C.

**N-2-(1*H*-Indol-3-yl)-2-oxoethyl-2-(3,4,5-trimethoxyphenyl)acetamide (13)**. Oxidation was done with dichlorodicyanoquinone (DDQ).<sup>50</sup> GC-MS for C<sub>21</sub>H<sub>22</sub>N<sub>2</sub>O<sub>5</sub>, 381.2 [M - H]<sup>+</sup>; mp 191.1 °C.

**3-[2-(3,4,5-Trimethoxybenzyl)-1,3-oxazol-5-yl]-1*H*-indole (14)**. LC-MS for C<sub>21</sub>H<sub>20</sub>N<sub>2</sub>O<sub>4</sub>, 365.3 [M + H]<sup>+</sup>; mp 171.1 °C; HRMS *m/z* = 364.140 60, calculated 364.142 281; purity HPLC 100%, *t*<sub>R</sub> = 8.767 min. Crystal structure of **14** has been proven by X-ray analysis: CAD4 Enraf Nonius, Cu K $\alpha$ , SIR-92, SHELXL-97, CCDC No. 680820. Further details of the crystal structure analysis are available in Supporting Information.

**N-2-(N-[2-(1-[[2-(Trimethylsilyl)ethoxy]methyl]-1*H*-indol-3-yl)-2-oxoethyl]-2-(3,4,5-trimethoxyphenyl)acetamide (15)**. LC-MS for C<sub>39</sub>H<sub>62</sub>N<sub>2</sub>O<sub>5</sub>Si<sub>2</sub> (*m/z* 695.1), 695.5 [M<sup>+</sup>]; mp 131.5 °C. Crystal structure of **15** has been proven by X-ray analysis.<sup>38</sup> Further details of the crystal structure analysis are available in Supporting Information.

**N-2-(1-Phenylsulfonyl-1*H*-indol-3-yl)-2-oxoethyl-2-(3,4,5-trimethoxyphenyl)acetamide (16)**. LC-MS for C<sub>27</sub>H<sub>26</sub>N<sub>2</sub>O<sub>7</sub>S, 523.0 [M + H]<sup>+</sup>; mp 151.6 °C.

**3-[1-(Phenylsulfonyl)-1*H*-indol-3-yl]-4-(3,4,5-trimethoxyphenyl)-1*H*-pyrrole-2,5-dione (17)**. LC-MS for C<sub>27</sub>H<sub>22</sub>N<sub>2</sub>O<sub>7</sub>S (*m/z* 522.1), 522 [M]<sup>+</sup>.

**N-(2-Oxo-2-(1-(2-(trimethylsilyl)ethoxy)methyl)-1*H*-indol-3-yl)-ethyl-2-(3,4,5-trimethoxyphenyl)acetamide (18)**. LC-MS for C<sub>27</sub>H<sub>36</sub>N<sub>2</sub>O<sub>6</sub>Si (*m/z* 512), 513 [M + H]<sup>+</sup>; mp 126.7 °C.

**3-(3,4,5-Trimethoxyphenyl)-4-(1-[[2-(trimethylsilyl)ethoxy]methyl]-1*H*-indol-3-yl)-1,5-dihydro-2*H*-pyrrole-2-one (19)**. LC-MS for C<sub>27</sub>H<sub>34</sub>N<sub>2</sub>O<sub>5</sub>Si (*m/z* 494), 495 [M + H]<sup>+</sup>; mp 115.8 °C; HRMS *m/z* = 494.222 30, calculated 494.223 672; purity HPLC 98.6%, *t*<sub>R</sub> = 10.782 min. Crystal structure of **19** has been proven by X-ray analysis: CAD4 Enraf Nonius, Cu K $\alpha$ , SIR-92, SHELXL-97, CCDC No. 680821. Further details of the crystal structure analysis are available in Supporting Information.

**3-(3,4,5-Trimethoxyphenyl)-4-(1-[[2-(trimethylsilyl)ethoxy]methyl]-1*H*-indol-3-yl)-1*H*-pyrrole-2,5-dione (19a)**. LC-MS for C<sub>27</sub>H<sub>32</sub>N<sub>2</sub>O<sub>6</sub>Si (*m/z* 808.6), 507.1 [M - H]<sup>+</sup>; mp >250 °C dec.

**4-(1*H*-Indol-3-yl)-3-(3,4,5-trimethoxyphenyl)-1*H*-pyrrole-2(5*H*)-one (1)**. Compound **19a** (120 mg, 0.24 mmol) was dissolved in 10 mL of DMF and 0.5 mL of ethylenediamine and heated to reflux when 1 mL of a 1 M TBAF solution in THF was added. After 2 h, the mixture was cooled to room temperature and quenched with saturated NH<sub>4</sub>Cl solution and extracted by ethyl acetate. The organic phase separated, dried over Na<sub>2</sub>SO<sub>4</sub>, and evaporated. The product was purified by flash chromatography on silica gel to yield 72%

65 mg (0.17 mmol) of **1** as an orange solid (which was identical to a sample of **1** from our earlier study<sup>20</sup>).

**4-[1-(Hydroxymethyl)-1*H*-indol-3-yl]-3-(3,4,5-trimethoxyphenyl)-1,5-dihydro-2*H*-pyrrole-2-one (20)**. LC-MS for C<sub>22</sub>H<sub>22</sub>N<sub>2</sub>O<sub>5</sub> (*m/z* 394.4), 395 [M + H]<sup>+</sup>; mp 176.3 °C.

**4-[1-(Methoxymethyl)-1*H*-indol-3-yl]-3-(3,4,5-trimethoxyphenyl)-1,5-dihydro-2*H*-pyrrole-2-one (21)**. LC-MS for C<sub>23</sub>H<sub>24</sub>N<sub>2</sub>O<sub>5</sub> (*m/z* 408.1), 409.1 [M + H]<sup>+</sup>; mp 194.6 °C; HRMS *m/z* = 408.167 41, calculated 408.168 491; purity HPLC 100%, *t*<sub>R</sub> = 7.763 min.

**4-[1-(Ethoxymethyl)-1*H*-indol-3-yl]-3-(3,4,5-trimethoxyphenyl)-1,5-dihydro-2*H*-pyrrole-2-one (22)**. LC-MS for C<sub>24</sub>H<sub>26</sub>N<sub>2</sub>O<sub>5</sub> (*m/z* 422.5), 423.1 [M + H]<sup>+</sup>; mp 167.1 °C; HRMS *m/z* = 422.183 11, calculated 422.184 141; purity HPLC 97.2%, *t*<sub>R</sub> = 8.428 min.

**4-[1-(Isopropoxymethyl)-1*H*-indol-3-yl]-3-(3,4,5-trimethoxyphenyl)-1,5-dihydro-2*H*-pyrrole-2-one (23)**. LC-MS for C<sub>25</sub>H<sub>28</sub>N<sub>2</sub>O<sub>5</sub> (*m/z* 436.5), 437.1 [M + H]<sup>+</sup>; mp 172.7 °C; HRMS *m/z* = 436.200 59, calculated 436.199 791; purity HPLC 98.5%, *t*<sub>R</sub> = 9.036 min. Crystal structure of **23** has been proven by X-ray analysis: CAD4 Enraf Nonius, Cu K $\alpha$ , SIR-92, SHELXL-97, CCDC No. 680822. Further details of the crystal structure analysis are available in Supporting Information.

**4-[1-(*tert*-Butoxymethyl)-1*H*-indol-3-yl]-3-(3,4,5-trimethoxyphenyl)-1,5-dihydro-2*H*-pyrrole-2-one (24)**. The compound was obtained in a procedure described for **20**. It was purified by flash chromatography to yield 16% of compound **24** as a brownish solid (for chromatogram, see Supporting Information). LC-MS for C<sub>26</sub>H<sub>30</sub>N<sub>2</sub>O<sub>5</sub> (*m/z* 450.5), 451.1 [M + H]<sup>+</sup>; mp 193.0 °C; HRMS *m/z* = 450.213 02, calculated 450.215 441; purity HPLC 98.8%, *t*<sub>R</sub> = 9.50 min. Crystal structure of **24** has been proven by X-ray analysis: CAD4 Enraf Nonius, Cu K $\alpha$ , SIR-92, SHELXL-97, CCDC No. 680823. Further details of the crystal structure analysis are available in Supporting Information.

**4-[1-(Phenoxymethyl)-1*H*-indol-3-yl]-3-(3,4,5-trimethoxyphenyl)-1,5-dihydro-2*H*-pyrrole-2-one (25)**. LC-MS for C<sub>28</sub>H<sub>26</sub>N<sub>2</sub>O<sub>5</sub> (*m/z* 470.5), 471.1 [M + H]<sup>+</sup>; mp 226.7 °C; HRMS *m/z* = 470.183 43, calculated 470.184 141; purity HPLC 76.5%, *t*<sub>R</sub> = 9.204 min.

**4-[1-[(Benzyloxy)methyl]-1*H*-indol-3-yl]-3-(3,4,5-trimethoxyphenyl)-1,5-dihydro-2*H*-pyrrole-2-one (26)**. LC-MS for C<sub>29</sub>H<sub>28</sub>N<sub>2</sub>O<sub>5</sub> (*m/z* 484.5), 485.1 [M + H]<sup>+</sup>; mp 65.0 °C; HRMS *m/z* = 484.196 83, calculated 484.199 791; purity HPLC 98.2%, *t*<sub>R</sub> = 9.772 min.

**N-2-(N-[(2,2-Dimethyl-1,3-dioxolan-4-yl)methyl]-1*H*-indol-3-yl)-2-oxoethyl-2-(3,4,5-trimethoxyphenyl)acetamide (27)**. LC-MS for C<sub>27</sub>H<sub>32</sub>N<sub>2</sub>O<sub>7</sub> (*m/z* 496.55), 497.0 [M + H]<sup>+</sup>.

**4-[1-[(2,2-Dimethyl-1,3-dioxolan-4-yl)methyl]-1*H*-indol-3-yl]-3-(3,4,5-trimethoxyphenyl)-1,5-dihydro-2*H*-pyrrole-2-one (28)**. The compound was prepared from 700 mg of **27** following a general procedure. Yield after flash chromatography purification (for chromatogram, see Supporting Information) was 73% as yellow solid. LC-MS for C<sub>27</sub>H<sub>30</sub>N<sub>2</sub>O<sub>6</sub> (*m/z* 478.54), 479.2 [M + H]<sup>+</sup>; mp 118.8 °C; HRMS *m/z* = 478.209 83, calculated 478.210 352; purity HPLC 98.4%, *t*<sub>R</sub> = 8.579 min.

**4-[1-(2,3-Dihydroxypropyl)-1*H*-indol-3-yl]-3-(3,4,5-trimethoxyphenyl)-1,5-dihydro-2*H*-pyrrole-2-one (29)**. LC-MS and FAB-MS for C<sub>24</sub>H<sub>26</sub>N<sub>2</sub>O<sub>6</sub> (*m/z* 438.47), 439.2 [M + H]<sup>+</sup>; mp 177.5 °C; HRMS *m/z* = 438.177 10, calculated 438.179 052; purity HPLC 97.1%, *t*<sub>R</sub> = 5.790 min.

**2-(N-Methyl-1*H*-indol-3-yl)-N-[2-(3,4,5-trimethoxyphenyl)-2-oxoethyl]acetamide (30)**. FAB-MS for C<sub>22</sub>H<sub>24</sub>N<sub>2</sub>O<sub>5</sub>, 397.2 [M + H]<sup>+</sup>; mp 130.6 °C.

**3-(N-Methyl-1*H*-indol-3-yl)-4-(3,4,5-trimethoxyphenyl)-1,5-dihydro-2*H*-pyrrole-2-one (31)**. The compound was prepared from 500 mg (1.26 mmol) of **30** following general procedure. The product precipitated from ethyl acetate to yield 73% 320 mg (0.85 mmol) of **31** as yellowish solid. FAB-MS for C<sub>22</sub>H<sub>22</sub>N<sub>2</sub>O<sub>4</sub>, 378.2 [M<sup>+</sup>]; mp 204.4 °C; HRMS *m/z* = 378.155 40, calculated 378.157 931; purity HPLC 97.4%, *t*<sub>R</sub> = 7.908 min.



**2-(1H-Indol-3-yl)-N-[2-(4-methoxyphenyl)2-oxoethyl]acetamide (32).** FAB-MS for  $C_{19}H_{18}N_2O_3$ , 323.2  $[M + H^+]$ ; mp 147.7 °C. Crystal structure of **32** has been proven by X-ray analysis: CAD4 Enraf Nonius, Cu K $\alpha$ , SIR-92, SHELXL-97, CCDC No. 680824. Further details of the crystal structure analysis are available in Supporting Information.

**3-(1H-Indol-3-yl)-4-(4-methoxyphenyl)-1,5-dihydro-2H-pyrrole-2-one (33).** FAB-MS for  $C_{19}H_{16}N_2O_2$ , 304.1  $[M^+]$ ; mp 260.4 °C; HRMS  $m/z$  = 304.118 63, calculated 304.121 161; purity HPLC 97.9%,  $t_R$  = 7.816 min. Crystal structure of **33** has been proven by X-ray analysis: CAD4 Enraf Nonius, Cu K $\alpha$ , SIR-92, SHELXL-97, CCDC No. 680825. Further details of the crystal structure analysis are available in Supporting Information.

**2-(N-Methyl-1H-indol-3-yl)-N-[2-(4-methoxyphenyl)2-oxoethyl]acetamide (34).** FAB-MS for  $C_{20}H_{20}N_2O_3$ , 337.2  $[M + H^+]$ ; mp 114.1 °C.

**3-(N-Methyl-1H-indol-3-yl)-4-(4-methoxyphenyl)-1,5-dihydro-2H-pyrrole-2-one (35).** The compound was prepared from 170 mg (0.5 mmol) of **34** following a general procedure. The product was purified by flash chromatography to yield (56%) 90 mg (0.28 mmol) of **35** as slightly ginger solid. FAB-MS for  $C_{20}H_{18}N_2O_2$ , 319.2  $[M + H^+]$ ; mp 203.0 °C; HRMS  $m/z$  = 318.138 50, calculated 318.136 811; purity HPLC 100%,  $t_R$  = 8.854 min. Crystal structure of **35** has been proven by X-ray analysis: CAD4 Enraf Nonius, Cu K $\alpha$ , SIR-92, SHELXL-97, CCDC No. 680826. Further details of the crystal structure analysis are available in Supporting Information.

**Selectivity Profiling of Compounds by IC<sub>50</sub> Values Using 24 Protein Kinases. Recombinant Protein Kinases.** The inhibitory profile of compounds was determined using the following 24 protein kinases (GenBankAcc.No. available on <http://www.proqinase.com/pages/science>): AKT1, ARK5, Aurora-A, Aurora-B, B-Raf-VE, CDK2/CycA, CDK4/CycD1, CK2-A1, EGF-R, EPHB4, ERBB2, FAK, IGF1-R, SRC, VEGF-R2, VEGF-R3, FLT3, INS-R, MET, PDGFR $\beta$ , PLK1, SAK, TIE2, COT (name as listed in the literature<sup>51</sup>).

All protein kinases were expressed using human cDNAs in Sf9 insect cells as recombinant GST-fusion proteins or His-tagged proteins by means of the baculovirus expression system. Kinases were purified by affinity chromatography using either GSH-agarose (Sigma) or Ni-NTH-agarose (Qiagen). The purity and identity of each kinase were checked by SDS-PAGE/silver staining and by Western blot analysis with specific antibodies.

**Protein Kinase Assay.** A proprietary protein kinase assay (33PanQinase activity assay) was used for measuring the kinase activity of the 24 protein kinases. All kinase assays were performed in 96-well FlashPlates from Perkin-Elmer/NEN (Boston, MA) in a 50  $\mu$ L reaction volume.

The assay for all enzymes contained 60 mM HEPES-NaOH, pH 7.5, 3 mM MgCl<sub>2</sub>, 3 mM MnCl<sub>2</sub>, 3  $\mu$ M sodium orthovanadate, 1.2 mM DTT, 50  $\mu$ g/mL PEG20000, 1  $\mu$ M [ $\gamma$ -33P]ATP (approximately  $5 \times 10^5$  cpm per well), and recombinant protein kinase (50–400 ng). Depending on the kinase, the following substrate-proteins were used: AKT1 (GSK3/14-27), ARK5 (autophosphorylation), Aurora-A, Aurora-B (Tetra(LRRWSLGG)), B-Raf-VE (MEK1 KM), CDK2/CycA (histone H1), CDK4/CycD1 (Rb-CTF), CK2-A1 (casein), EGF-R, EPHB4, ERBB2, FAK, IGF1-R, SRC, VEGF-R2, VEGF-R3 (poly(Glu,Tyr) 4:1), FLT3, INS-R, MET, PDGFR $\beta$  (poly(Ala,Glu,Lys,Tyr) 6:2:5:1), PLK1 (casein), SAK (autophosphorylation), TIE2 (poly(Glu,Tyr) 4:1), COT (autophosphorylation).

The IC<sub>50</sub> values were measured by testing 10 concentrations of compounds. The final DMSO concentration in the assay was 1%. The reaction cocktails were incubated at 30 °C for 80 min. The reaction was stopped with 50  $\mu$ L of 2% (v/v) H<sub>3</sub>PO<sub>4</sub>. Plates were aspirated and washed two times with 200  $\mu$ L of 0.9% (w/v) NaCl. Incorporation of 33P<sub>i</sub> was determined with a microplate scintillation counter (Microbeta Trilux, Wallac). All assays were performed with a BeckmanCoulter/Sagian robotic system.

**In Vitro Angiogenesis Assay.** The in vitro sprouting angiogenesis assay was performed as described previously.<sup>52</sup> Briefly, human lung-derived microvascular endothelial cells (HLMVEC) were seeded on cytodex-3 microcarrier beads and embedded into a three-dimensional fibrinogen gel containing 20 ng/mL VEGF either alone or in combina-

tion with the different test compounds. From a stem solution of the compounds (concentration of 1 mM in DMSO), an amount of 2  $\mu$ L was dissolved in 1.5 mL of gel to give a final compound concentration of 1.3  $\mu$ M in the assay (the data in Supporting Information additionally show the results for testing the compounds at a final assay concentration of 2.6  $\mu$ M). Fibrinogen gels without growth factors served as a negative control. Polymerization of fibrin gels was started by adding 0.65 U/mL thrombin. Afterward, gels were incubated in MCDB131 containing the appropriate concentrations of factors, 5% FCS, 5% human serum, and 200 U/mL Trasylol (Bayer Leverkusen, Germany). After 24 h the gel was fixed in 1% PFA and the number of sprouts per 50 beads was counted by microscope. The assay was performed in triplets per condition (final number of different experiments  $n$  = 9) and statistically analyzed.

**Apoptose Assay.** Human dermal microvascular endothelial cells (HDMECs) were incubated with appropriate concentrations of the compounds for 24 h; adherent cells and the supernatant were harvested for detection of apoptotic cells by cleaved caspase-3 staining with a specific antibody (Cell Signaling, Danvers, MA) and subsequent FACS analysis. Staurosporine-treated HDMECs (5 h, 2.1  $\mu$ M) served as a positive control. The experiment was repeated three times.

**Molecular Modeling.** All modeling was performed on a Red Hat Linux system. For visualization and building of the structures, SYBYL 7.2.3 was used. The Connolly surface was calculated using the MOLCAD module in Sybyl and colored according to the lipophilicity (from very hydrophobic to hydrophilic corresponds to brown to green to blue). Compound **2** was docked into the active site of VEGFR-2 using the FlexX docking program.<sup>53</sup> The FlexX scoring function was applied during the placement and construction phase of the ligands and DrugScore for the final ranking.<sup>54</sup> The 3D coordinates of the VEGFR-2 catalytic core in complex with a 2-anilino-5-aryloxazole inhibitor were taken from the Brookhaven Protein Databank (PDB code 1Y6A).<sup>17</sup>

**Acknowledgment.** We thank Susanne Weidemann, Department of Dermatology, University of Tübingen, for her helpful assistance in performing the cellular assays. Financial support by Merckle GmbH, Blaubeuren, is gratefully acknowledged.

**Supporting Information Available:** (1) IR data, (2) <sup>1</sup>H and <sup>13</sup>C NMR data, (3) purification data of compounds **2**, **13**, **19**, **20**, **23–28** by flashchromatography, (4) purity of key target compounds, (5) X-ray analysis results for compounds **1**, **2**, **4**, **6a**, **11**, **14**, **15**, **19**, **23**, **24**, **32**, **33**, and **35**, (6) quality parameters for the protein kinase assay (IC<sub>50</sub> values at 24 protein kinases), and (7) details of HLMVEC sprouting assay of compounds **1–3** at 2.6  $\mu$ M. This material is available free of charge via the Internet at <http://pubs.acs.org>.

## References

- (1) Kiselyov, A.; Balakin, K. V.; Tkachenko, S. E. VEGF/VEGFR signalling as a target for inhibiting angiogenesis. *Expert Opin. Invest. Drugs* **2007**, *16*, 83–107.
- (2) Shibuya, M. Differential roles of vascular endothelial growth factor receptor-1 and receptor-2 in angiogenesis. *J. Biochem. Mol. Biol.* **2006**, *39*, 469–478.
- (3) Goldman, J.; Rutkowski, J. M.; Shields, J. D.; Pasquier, M. C.; Cui, Y.; Schmokel, H. G.; Willey, S.; Hicklin, D. J.; Pytowski, B.; Swartz, M. A. Cooperative and redundant roles of VEGFR-2 and VEGFR-3 signaling in adult lymphangiogenesis. *FASEB J.* **2007**, *21*, 1003–1012.
- (4) Laakkonen, P.; Waltari, M.; Holopainen, T.; Takahashi, T.; Pytowski, B.; Steiner, P.; Hicklin, D.; Persaud, K.; Tonra, J. R.; Witte, L.; Alitalo, K. Vascular endothelial growth factor receptor 3 is involved in tumor angiogenesis and growth. *Cancer Res.* **2007**, *67*, 593–599.
- (5) Schenone, S.; Bondavalli, F.; Botta, M. Antiangiogenic agents: an update on small molecule VEGFR inhibitors. *Curr. Med. Chem.* **2007**, *14*, 2495–2516.
- (6) Hicklin, D. J.; Ellis, L. M. Role of the vascular endothelial growth factor pathway in tumor growth and angiogenesis. *J. Clin. Oncol.* **2005**, *23*, 1011–1027.
- (7) Gollob, J. A.; Wilhelm, S.; Carter, C.; Kelley, S. L. Role of Raf kinase in cancer: therapeutic potential of targeting the Raf/MEK/ERK signal transduction pathway. *Semin. Oncol.* **2006**, *33*, 392–406.

- (8) Mirshahi, P.; Toprak, S. K.; Faussat, A. M.; Dubrulle, S.; Marie, J. P.; Soria, C.; Soria, J.; Mirshahi, M. Malignant hematopoietic cells induce an increased expression of VEGFR-1 and VEGFR-3 on bone marrow endothelial cells via AKT and mTOR signalling pathways. *Biochem. Biophys. Res. Commun.* **2006**, *349*, 1003–1010.
- (9) Manetti, F.; Botta, M. Small-molecule inhibitors of fibroblast growth factor receptor (FGFR) tyrosine kinases (TK). *Curr. Pharm. Des.* **2003**, *9*, 567–581.
- (10) Prien, O. The gatekeeper: friend or foe in identifying the next generation of kinase inhibitors. *ChemMedChem* **2006**, *1*, 1195–1196.
- (11) Arnold, D.; Peinert, S.; Voigt, W.; Schmoll, H. J. Epidermal growth factor receptor tyrosine kinase inhibitors: present and future role in gastrointestinal cancer treatment: a review. *Oncologist* **2006**, *11*, 602–611.
- (12) Lewis, N. L. The platelet-derived growth factor receptor as a therapeutic target. *Curr. Oncol. Rep.* **2007**, *9*, 89–95.
- (13) Medinger, M.; Dreys, J. Receptor tyrosine kinases and anticancer therapy. *Curr. Pharm. Des.* **2005**, *11*, 1139–1149.
- (14) (a) Bain, J.; McLauchlan, H.; Elliott, M.; Cohen, P. The specificities of protein kinase inhibitors: an update. *Biochem. J.* **2003**, *371*, 199–204. (b) Bain, J.; Plater, L.; Elliott, M.; Shpiro, N.; Hastie, J.; McLauchlan, H.; Klevernic, I.; Arthur, S.; Alessi, D.; Cohen, P. The selectivity of protein kinase inhibitors: a further update. *Biochem. J.* **2007**, *408*, 297–315.
- (15) Fabian, M. A.; Biggs, W. H., III; Treiber, D. K.; Atteridge, C. E.; Azimioara, M. D.; Benedetti, M. G.; Carter, T. A.; Ciceri, P.; Edeen, P. T.; Floyd, M.; Ford, J. M.; Galvin, M.; Gerlach, J. L.; Grotzfeld, R. M.; Herrgard, S.; Insko, D. E.; Insko, M. A.; Lai, A. G.; Lias, J. M.; Mehta, S. A.; Milanov, Z. V.; Velasco, A. M.; Wodicka, L. M.; Patel, H. K.; Zarrinkar, P. P.; Lockhart, D. J. A small molecule-kinase interaction map for clinical kinase inhibitors. *Nat. Biotechnol.* **2005**, *23*, 329–336.
- (16) (a) <http://www.insightpharmareports.com/>. (b) Peifer, C.; Krasowski, A.; Haemmerle, N.; Kohlbacher, O.; Dannhardt, G.; Totzke, F.; Schaechtele, C.; Laufer, S. Profile and molecular modeling of 3-(indole-3-yl)-4-(3,4,5-trimethoxyphenyl)-1H-pyrrole-2,5-dione (I) as a highly selective VEGF-R2/3 inhibitor. *J. Med. Chem.* **2006**, *49*, 7549–7553.
- (17) Harris, P. A.; Cheung, M.; Hunter, R. N.; Brown, M. L.; Veal, J. M.; Nolte, R. T.; Wang, L.; Liu, W.; Crosby, R. M.; Johnson, J. H.; Epperly, A. H.; Kumar, R.; Luttrell, D. K.; Stafford, J. A. Discovery and evaluation of 2-anilino-5-aryloxazoles as a novel class of VEGFR2 kinase inhibitors. *J. Med. Chem.* **2005**, *48*, 1610–1619.
- (18) Babu, P. R.; Balasubramanian, T. R. A simple and convenient synthesis of 3,4-diaryl-1,5-dihydro-2H-pyrrol-2-ones. *Indian J. Chem. B* **1987**, *26*, 63.
- (19) Coffin, A. R.; Roussel, M. A.; Tserlin, E.; Pelkey, E. T. Regiocontrolled synthesis of pyrrole-2-carboxaldehydes and 3-pyrrolin-2-ones from pyrrole Weinreb amides. *J. Org. Chem.* **2006**, *71*, 6678–6681.
- (20) Peifer, C.; Stoiber, T.; Unger, E.; Totzke, F.; Schaechtele, C.; Marmé, D.; Brenk, R.; Klebe, G.; Schollmeyer, D.; Dannhardt, G. Design, synthesis, and biological evaluation of 3,4-diarylmaleimides as angiogenesis inhibitors. *J. Med. Chem.* **2006**, *49*, 1271–1281.
- (21) O'Neill, D. J.; Shen, L.; Prouty, C.; Conway, B. R.; Westover, L.; Xu, J. Z.; Zhang, H. C.; Maryanoff, B. E.; Murray, W. V.; Demarest, K. T.; Kuo, G. H. Design, synthesis, and biological evaluation of novel 7-azaindolyheteroaryl-maleimides as potent and selective glycogen synthase kinase-3 $\beta$  (GSK-3 $\beta$ ) inhibitors. *Bioorg. Med. Chem.* **2004**, *12*, 3167–3185.
- (22) Davis, P. D.; Hill, C. H.; Lawton, G.; Nixon, J. S.; Wilkinson, S. E.; Hurst, S. A.; Keech, E.; Turner, S. E. Inhibitors of protein kinase C. I. 2,3-Bisarylmaleimides. *J. Med. Chem.* **1992**, *35*, 177–184.
- (23) Wood, J. L.; Stoltz, B. M.; Dietrich, H. J. Total synthesis of (+)- and (–)-K252a. *J. Am. Chem. Soc.* **1995**, *117*, 10413–10414.
- (24) Becknell, N. C.; Zulli, A. L.; Angeles, T. S.; Yang, S.; Albom, M. S.; Aimone, L. D.; Robinson, C.; Chang, H.; Hudkins, R. L. Novel C-3 N-urea, amide, and carbamate dihydroindazolo[5,4-a]pyrrolo[3,4-c]carbazole analogs as potent TIE-2 and VEGF-R2 dual inhibitors. *Bioorg. Med. Chem. Lett.* **2006**, *16*, 5368–5372.
- (25) Link, J. T.; Raghavan, S.; Gallant, M.; Danishefsky, S. J.; Chou, T. C.; Ballas, L. M. Staurosporine and ent-staurosporine: the first total syntheses, prospects for a regioselective approach, and activity profiles. *J. Am. Chem. Soc.* **1996**, *118*, 2825–2842.
- (26) Bregman, H.; Williams, D. S.; Meggers, E. Pyrido[2,3-a]pyrrolo[3,4-c]carbazole-5,7(6H)-diones: synthesis, cyclometalation, and protein kinase inhibition. *Synthesis* **2005**, *9*, 1521–1527.
- (27) Li, K.; Hamann, L. G.; Koreeda, M. A convenient, highly stereoselective synthesis of anti-a,b-epoxy alcohols by the Luche reduction of a,b-epoxy ketones. *Tetrahedron Lett.* **1992**, *33*, 6569–6570.
- (28) Link, J. T.; Danishefsky, S. J. Regioselective imide reduction: an issue in the total synthesis of staurosporine. *Tetrahedron Lett.* **1994**, *35*, 9135–9138.
- (29) Harrington-Frost, N. M.; Pattenden, G. A new synthesis of pentalenene using a novel tandem cyclisation involving ketene radical intermediates. *Tetrahedron Lett.* **2000**, *41*, 403–405.
- (30) Fuerstner, A.; Hupperts, A. Carbonyl coupling reactions catalytic in titanium and the use of commercial titanium powder for organic synthesis. *J. Am. Chem. Soc.* **1995**, *117*, 4468–4475.
- (31) Fuerstner, A.; Tesche, B. Chemical impact on a seemingly “inert” material: an electron microscopic case study of titanium activated by chlorosilanes. *Chem. Mater.* **1998**, *10*, 1968–1973.
- (32) Ephritikhine, M. A new look at the McMurry reaction. *Chem. Commun.* **1998**, *23*, 2549–2554.
- (33) Eils, S.; Winterfeldt, E. Complete regioselectivity in staurosporine chromophore formation. *Synthesis* **1999**, *2*, 275–281.
- (34) Piers, E.; Britton, R.; Andersen, R. J. Improved synthesis of isogranulatimide, a G2 checkpoint inhibitor. Syntheses of didemnimide C, isodidemnimide A, neodidemnimide A, 17-methylgranulatimide, and isogranulatimides A–C. *J. Org. Chem.* **2000**, *65*, 530–535.
- (35) Roy, S.; Haque, S.; Gribble, G. W. Synthesis of novel oxazolyl-indoles. *Synthesis* **2006**, *23*, 3948–3954.
- (36) LaMattina, J. L. Reaction of  $\alpha$ -amino ketone hydrochlorides with ortho esters: an oxazole synthesis. *J. Org. Chem.* **1980**, *45*, 2261–2262.
- (37) Vereshchagin, A. L.; Pogodaeva, N. N.; Semenov, A. A. Acid–base properties of indolylglyoxal and some acetylindoles. *Khim. Geterotsikl.* **1987**, *12*, 1621–1624.
- (38) Peifer, C.; Selig, R.; Schollmeyer, D.; Laufer, S. *N*-(Z)-2-[1-(Triisopropylsilyl)-1H-indol-3-yl]-2-trisopropylsilyloxyvinyl]-2-(3,4,5-trimethoxyphenyl)acetamide. *Acta Crystallogr. E* **2007**, *63*, 1266–1268.
- (39) Labadie, S. S.; Teng, E. Indol-2-yltributylstannane: a versatile reagent for 2-substituted indoles. *J. Org. Chem.* **1994**, *59*, 4250–4254.
- (40) Diez-Martin, D.; Kotecha, N. R.; Ley, S. V.; Mantegani, S.; Menendez, J. C.; Organ, H. M.; White, A. D.; Banks, B. J. Total synthesis of the ionophore antibiotic CP-61,405 (rouniennocin). *Tetrahedron* **1992**, *48*, 7899–7938.
- (41) Barril, X.; Morley, S. D. Unveiling the full potential of flexible receptor docking using multiple crystallographic structures. *J. Med. Chem.* **2005**, *48*, 4432–4443.
- (42) Gervasio, F. L.; Laio, A.; Parrinello, M. Flexible docking in solution using metadynamics. *J. Am. Chem. Soc.* **2005**, *127*, 2600–2607.
- (43) Muegge, I.; Enyedy, I. J. Virtual screening for kinase targets. *Curr. Med. Chem.* **2004**, *11*, 693–707.
- (44) Stommel, J. M.; Kimmelman, A. C.; Ying, H.; Nabioullin, R.; Ponugoti, A. H.; Wiedemeyer, R.; Stegh, A. H.; Bradner, J. E.; Ligon, K. L.; Brennan, C.; Chin, L.; DePinho, R. A. Coactivation of receptor tyrosine kinases affects the response of tumor cells to targeted therapies. *Science* **2007**, *318*, 287–290.
- (45) Engel, G. L.; Farid, N. A.; Faul, M. M.; Richardson, L. A.; Winneroski, L. L. Salt form selection and characterization of LY335351 mesylate monohydrate. *Int. J. Pharm.* **2000**, *198*, 239–247.
- (46) Yilmaz, A.; Kliche, S.; Mayr-Beyrle, U.; Fellbrich, G.; Waltenberger, J. p38 MAPK inhibition is critically involved in VEGFR-2-mediated endothelial cell survival. *Biochem. Biophys. Res. Commun.* **2003**, *306*, 730–736.
- (47) Solovyan, V. T.; Keski-Oja, J. Apoptosis of human endothelial cells is accompanied by proteolytic processing of latent TGF- $\beta$  binding proteins and activation of TGF- $\beta$ . *Cell Death Differ.* **2005**, *12*, 815–826.
- (48) Dubowchik, G. M.; Vruthula, V. M.; Dasgupta, B.; Ditta, J.; Chen, T.; Sheriff, S.; Sipman, K.; Witmer, M.; Tredup, J.; Vyas, D. M.; Verdoorn, T. A.; Bollini, S.; Vinitsky, A. 2-Aryl-2,2-difluoroacetamide FKBP12 ligands: synthesis and X-ray structural studies. *Org. Lett.* **2001**, *3*, 3987–3990.
- (49) Iakovou, K.; Varvaresou, A.; Kourounakis, A. P.; Stead, K.; Sugden, D.; Tsotinis, A. Design, synthesis and biological evaluation of novel b-substituted indol-3-yl ethylamido melatonergic analogues. *J. Pharm. Pharmacol.* **2002**, *54*, 147–156.
- (50) Oikawa, Y.; Yonemitsu, O. Selective oxidation of the side chain at C-3 of indoles. *J. Org. Chem.* **1977**, *42*, 1213–1216.
- (51) Manning, G.; Whyte, D. B.; Martinez, R.; Hunter, T.; Sudarsanam, S. The protein kinase complement of the human genome. *Science* **2002**, *298*, 1912–1916.
- (52) Nehls, V.; Drenckhahn, D. A novel, microcarrier-based in vitro assay for rapid and reliable quantification of three-dimensional cell migration and angiogenesis. *Microvasc. Res.* **1995**, *50*, 311–322.
- (53) Rarey, M.; Kramer, B.; Lengauer, T.; Klebe, G. A fast flexible docking method using an incremental construction algorithm. *J. Mol. Biol.* **1996**, *261*, 470–489.
- (54) Gohlke, H.; Hendlich, M.; Klebe, G. Knowledge-based scoring function to predict protein–ligand interactions. *J. Mol. Biol.* **2000**, *295*, 337–356.